1999-05-01

Stratified Volume Diffractive Optical Elements as High Efficiency Gratings

Gregory P. Nordin
nordin@byu.edu

D. M. Chambers

Original Publication Citation
D. M. Chambers and G. P. Nordin, "Stratified Volume Diffractive Optical Elements as High Efficiency Gratings", J. Opt. Soc. Am. A 16(5), pp. 1168-1174 (1999)

Stratified volume diffractive optical elements as high-efficiency gratings

Diana M. Chambers*

Center for Applied Optics, The University of Alabama in Huntsville, Huntsville, Alabama 35899

Gregory P. Nordin

Department of Electrical and Computer Engineering, The University of Alabama at Huntsville, Huntsville, Alabama 35899

Received August 10, 1998; revised manuscript received January 15, 1999; accepted January 22, 1999

We propose stratified volume diffractive optical elements as a new type of diffractive optical element that is capable of functioning as a high-efficiency grating in applications with requirements not suited to traditional holographic or diffractive optical techniques. In this approach, diffractive optical fabrication methods are used to construct an optical structure that emulates volume grating behavior. We discuss the diffraction properties of stratified volume diffractive optical elements and compare them with those used previously in both volume holographic optical elements and stratified volume holographic optical elements. A systematic design process is then presented for deriving structure parameters. We illustrate this process by designing a prototype stratified volume diffractive optical element to meet the operational specifications for a beam-scanning element in a spaceborne coherent wind lidar. We use numerical simulation to assess the performance of the prototype element, including sensitivity to fabrication errors. © 1999 Optical Society of America [S0740-3232(99)01105-9]

OCIS codes: 050.2770, 050.1970, 050.7330, 090.1970, 090.7330.

1. INTRODUCTION

Gratings with high diffraction efficiency into a single order find use in a multitude of applications ranging from optical interconnects to beam steering. Such gratings have been realized with volume holographic, blazed, and diffractive optical techniques.[1–9] However, each of these methods has limitations that restrict the range of applications in which it can be used. For example, high-efficiency volume holographic gratings require an appropriate combination of thickness and permittivity modulation throughout the bulk of the material. Possible combinations of these parameters are limited by properties of currently available materials, thus restricting the range of potential applications. Similarly, fabrication considerations place constraints on the minimum achievable period for blazed gratings and multi-phase-level diffractive optical gratings, hence limiting the applications in which they can be used. Likewise, high diffraction efficiency can be achieved for deep binary gratings but only for specific incidence angles. In this paper we propose an alternative method for creating high-efficiency gratings that we call stratified volume diffractive optical elements (SVDOE's). In this approach diffractive optical techniques are used to create an optical structure that emulates volume grating behavior. This concept is derived from previous research in stratified volume holographic optical elements (SVHOE's) in which holographic recording materials available only as thin films were combined to create an element with diffraction efficiency approaching that of a traditional volume holographic optical element.[10–12]

In this paper we examine the diffraction properties of SVDOE's and illustrate their potential use as beam-scanning elements for space-based coherent wind lidar.[13] This application specifies a transmissive scanner element with a *normally* incident input beam and an exiting beam deflected at a fixed angle from the optical axis. A conical span pattern will be produced by rotation of the scanner element about the optical axis. The wavelength of the incident beam is approximately 2 μm, and the required deflection angle is 30°. Additional requirements include insensitivity to polarization orientation, minimal disruption of the transmitted wave front (as a result of the heterodyne detection system), low mass, and the ability to withstand launch and space environments.

The scanner function can in principle be achieved with a rotating prism. However, mass and satellite stability considerations make a thin holographic or diffractive element attractive. For either option, a grating period of approximately 4 μm is required. This is small enough that fabrication of appropriate high-efficiency blazed or multi-phase-level diffractive optical gratings is prohibitively difficult. Moreover, bulk or stratified volume holographic approaches appear impractical because of materials limitations at 2 μm and the need to maintain adequate wave-front quality. The requirement for normal-incidence operation likewise eliminates the use of deep binary gratings. In contrast to these traditional approaches, the SVDOE concept has the potential to satisfy lidar beam scanner requirements.

Our examination of SVDOE's begins in Section 2 with a discussion of SVDOE structure, modeling methodology,

0740-3232/99/051184-10$15.00

and basic diffraction properties. In Section 3 we develop design procedures. These are applied in Section 4 to a prototype beam-scanner design. We use numerical simulations to evaluate its predicted performance and to explore fabrication tolerances. Future research directions are discussed in Section 5.

2. STRATIFIED VOLUME DIFFRACTIVE OPTICAL ELEMENTS

A. Structure

The SVDOE structure consists of binary grating layers interleaved with homogeneous layers, as illustrated in Fig. 1. Ridges in the grating layers are composed of a high-refractive-index material, whereas the grooves and homogeneous layers utilize a material with a low refractive index. The binary grating layers modulate a wave front as it passes through the structure, and the homogeneous layers allow diffraction to occur. While the individual binary grating layers are relatively thin, incorporation of diffraction via the homogeneous layers permits a SVDOE to attain diffraction efficiencies comparable with those of a volume holographic element in which modulation and diffraction are spatially coincident throughout the medium.

Since the layers in this type of structure must be fabricated sequentially, the binary grating layers can be laterally shifted relative to one another (as illustrated in Fig. 1) to create a stratified diffractive optical structure analogous to a volume grating with slanted fringes. This ability of the layers to be shifted allows an element to be designed with high diffraction efficiency into the first order for any arbitrary angle of incidence (including normal incidence as is required by the lidar beam-scanner application).

B. Simulation Methodology

Several analysis methods based on scalar theory were previously applied to the simulation of SVHOE performance.[10–12,14] However, depending on the choice of materials, the grating structure discussed above can include a relatively large refractive-index difference between the materials in the grating layer. For the specific example application considered here, there is also a small period-to-wavelength ratio (e.g., <10). Accurate prediction of diffraction efficiency under these conditions requires a rigorous electromagnetic diffraction theory. Rigorous coupled-wave analysis (RCWA), as formulated by Moharam *et al.*,[15,16] was chosen to model the behavior of these stratified structures.

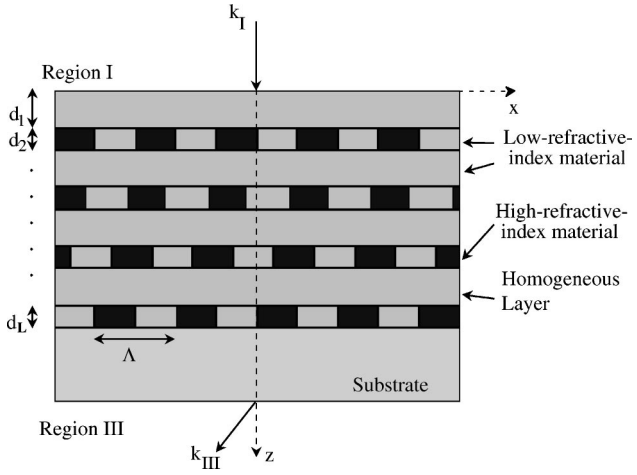

Fig. 1. Schematic illustration of the SVDOE structure.

This formulation of RCWA has evolved into an efficient and stable implementation for general multilayer structures from its inception for single-layer, planar gratings. The algorithm for planar gratings[17] was presented in a matrix form, based on the method of state variables, such that it could be easily implemented on a computer and solved with eigenfunction and eigenvalue library routines. The eigenvalue formulation of RCWA could be applied to the general case of slanted gratings, whereas a similar formulation of the rigorous modal approach was limited to unslanted gratings. Analysis of several grating configurations illustrated the improved accuracy of RCWA compared with several approximate theories.

Following its initial formulation in a state-variable representation, RCWA was then applied to the analysis of surface-relief gratings.[18] Arbitrary grating profiles were analyzed by dividing the grating into a large number of thin layers parallel to the substrate and treating each in sequence. For each thin layer the relative permittivity was expanded as a Fourier series, and then the rigorous coupled-wave equations were solved in that layer. Applying electromagnetic boundary conditions at the interface between successive layers ensured accurate analysis of the grating system. Comparison with other rigorous methods for sinusoidal surface-relief profiles showed excellent agreement for diffraction efficiencies while greater accuracy in conservation of power was maintained.

A subsequent formulation of RCWA[15] for single, binary gratings introduced simplifications to the coupled-wave equations, which enhanced computational efficiency and reduced computer memory requirements while maintaining its rigorous approach. Numerical overflow in the application of electromagnetic boundary conditions was eliminated by a normalization process that ensured that arguments of exponential functions were always negative. The stability of this approach was illustrated by calculation of diffraction efficiencies for gratings with depths of as much as 50 times the incident wavelength.

These improvements for single-layer binary gratings were applied to a RCWA formulation for analysis of multilayer surface-relief gratings.[16] However, numerical instabilities could still arise from the approach used in enforcing the electromagnetic boundary conditions at successive interfaces. The source of these instabilities, namely, evanescent fields, was thoroughly discussed by Moharam *et al.*,[16] and a solution involving an enhanced transmittance matrix approach was developed. The capabilities of the enhanced transmittance matrix algorithm were illustrated by analysis of a 16-level asymmetric grating for periods of 1 and 10 times the incident wavelength and for depths of as much as 50 times the incident wavelength. Diffraction efficiency for each of the grating configurations was calculated for planar diffraction in both TE and TM polarizations and for conical diffraction. In all cases, the conservation of power was ac-

curate to within one part in 10^{10}, and the solution converged with an increasing number of field harmonics, thus meeting the stated criteria for numerical stability.[16]

This RCWA implementation for analyzing multilayer gratings by the enhanced transmittance matrix approach was chosen as the starting point for an extended algorithm to accommodate the unique, layered structure of SVDOE's. Our extended algorithm for SVDOE's is outlined in this section, and full details for the specific case of planar diffraction for TE polarization are presented in Appendix A. We have also implemented formulations for TM polarization and for conical diffraction, using the same approach. We begin by establishing space-harmonic expansions for the fields in a homogeneous, or uniform, layer similar to the space-harmonic expansions in a grating layer. Then, using the matrix structure generated from applying electromagnetic boundary conditions for a binary grating as a basis, we enforce an identical matrix structure when matching boundary conditions for uniform layers. Given the identical matrix structure for all layer types, the sequence of grating and uniform layers may be completely arbitrary. Shifting of the grating layers to mimic slanted fringes is accommodated in the Fourier expansion of the relative permittivity for each grating layer such that lateral position is completely independent for all grating layers. Material properties, including both refractive index and dispersion, may be defined for the grooves and the ridges of each grating layer independently as well as for each homogeneous layer independently. The only assumption made in this algorithm is that all grating layers have identical period. In addition, we have also included in our algorithm the reformulation of the coupled-wave equations as published by Li[19] to improve convergence for TM polarization and conical diffraction.

Verification of the algorithm implementation was conducted with the same criteria as those of Moharam *et al.*,[15,16] i.e., conservation of power to within one part in 10^{10} and convergence with an increasing number of space harmonics. Several grating profiles studied in the references cited above, such as deep binary gratings and multilayer sawtooth configurations, were analyzed and were found to agree with published results and also to meet the conservation and convergence criteria.[15–17] A previously published nine-layer resonant grating configuration[20] consisting of a binary grating layer surrounded by high–low quarter-wave stacks was also studied since it contained both binary and uniform layers, similar to a SVDOE. The transmittance of the filter as a function of wavelength compared exactly to the published curve. A SVDOE structure consisting of five grating layers separated by uniform layers was then studied. As is shown in Fig. 2, convergence occurred within a very small number of retained space harmonics (<10) for both TE and TM polarizations. For all numbers of space harmonics the residual error in the conservation of power was of the order of 10^{-14}.

C. Diffraction Properties

Similar to that of SVHOE's, the stratified structure of SVDOE's introduces diffraction properties that are unique compared with the behavior of traditional volume holographic or diffractive optical gratings. We illustrate these properties in this section by examining the diffraction efficiency of SVDOE's as a function of the total grating layer thickness, the homogeneous layer thickness, and the incidence angle of the readout beam.

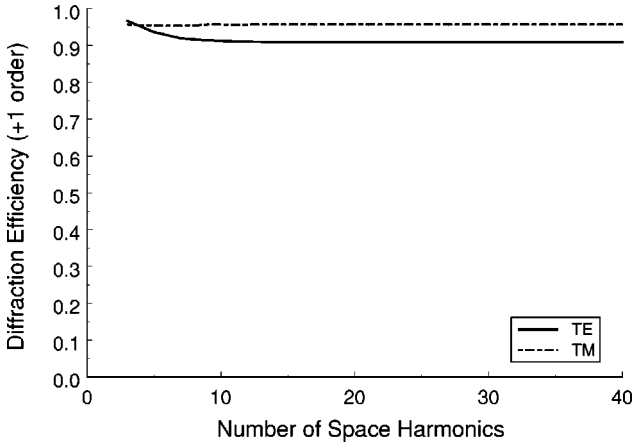

Fig. 2. Convergence of the diffraction efficiency as a function of the number of space harmonics retained in the calculation. $\lambda_0 = 2.06\ \mu$m, θ=9.885°, $n_{\mathrm{I}} = 1.5$, $n_{\mathrm{III}} = 1.5$, $n_{\mathrm{ridge}} = 2.0$, $n_{\mathrm{groove}} = 1.5$, $d_{\mathrm{grating}} = 0.638$, $d_{\mathrm{homogeneous}} = 4.6\ \mu$m.

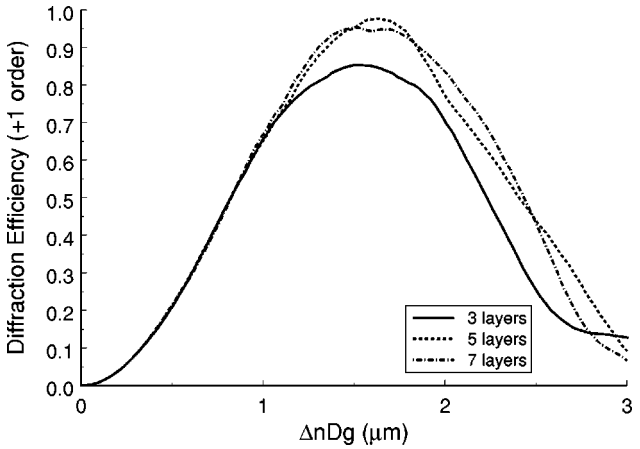

Fig. 3. Diffraction efficiency of a five-layer SVDOE as a function of total grating layer thickness ($\Delta n = 0.1$). $\lambda_0 = 2.06\ \mu$m, θ=9.885°, $n_{\mathrm{I}} = 1.5$, $n_{\mathrm{III}} = 1.5$, $n_{\mathrm{ridge}} = 1.6$, $n_{\mathrm{groove}} = 1.5$, $d_{\mathrm{homogeneous}} = 2.1\ \mu$m.

In a conventional grating the diffraction efficiency increases with increasing modulation thickness until it reaches a peak value, after which the diffraction efficiency decreases as the grating becomes overmodulated. We consider the behavior of SVDOE's in similar circumstances by defining a structure with constant homogeneous layer thickness and by varying grating layer thickness. The readout beam is positioned at Bragg incidence, with the grating layers aligned such that they have no lateral offset relative to one another. Figure 3 shows the +1-order diffraction behavior for SVDOE's consisting of three, five, and seven grating layers as a function of $\Delta n D_g$, in which Δn is the refractive-index difference between the ridge and the groove materials and D_g is the total grating layer thickness in each structure. For this case $\Delta n = 0.1$. The homogeneous layers are assumed to have a refractive index identical to the grating grooves.

Note that the diffraction efficiency follows the expected behavior, in which Fig. 3 shows the first period of an approximately sinusoidal dependence of the diffraction efficiency on the product $\Delta n D_g$. The peak diffraction efficiency is achieved for the same value of $\Delta n D_g$, ~1.5 μm, regardless of the number of grating layers.

To further examine this behavior, we consider another set of SVDOE's under the same conditions, but with $\Delta n = 0.5$. Typical results are shown in Fig. 4. Although there is now significant structure in the curves, the same general trends apply. In particular, note that the peak diffraction efficiency for each curve still occurs near a value of $\Delta n D_g \cong 1.5$ μm. The variations in the curves from a sinusoidal shape are due to interference from multiple reflections between the grating layers. As one would therefore expect, we observe that the structure in the curves changes significantly for small changes in the homogeneous layer thickness.

The same type of behavior seen in Fig. 3 was reported for SVHOE's[11] (for which small grating refractive-index modulation was assumed). In this case the grating strength ν was used to characterize the relationship of first-order diffraction efficiency to total modulation thickness, which was shown to follow the well-known $\sin^2(\nu/2)$ expression for Bragg incidence readout of dielectric volume holographic gratings. A general expression for $\nu/2$, which we will call χ, that is applicable to the case of sinusoidal dielectric transmission gratings was defined by Kogelnik[21] as

$$\chi = \frac{\kappa D_g}{\sqrt{c_R c_S}} = \frac{\pi \Delta n_{\text{amp}} D_g}{\lambda_0 \sqrt{c_R c_S}}, \tag{1}$$

in which $\kappa = \pi \Delta n_{\text{amp}}/\lambda_0$ describes the coupling between the zeroth and the first diffracted orders as they propagate through the bulk material, Δn_{amp} represents the amplitude of the sinusoidal refractive-index modulation, λ_0 is the free-space wavelength, and D_g is the total modulation thickness. The obliquity factors, c_R and c_S, are given by

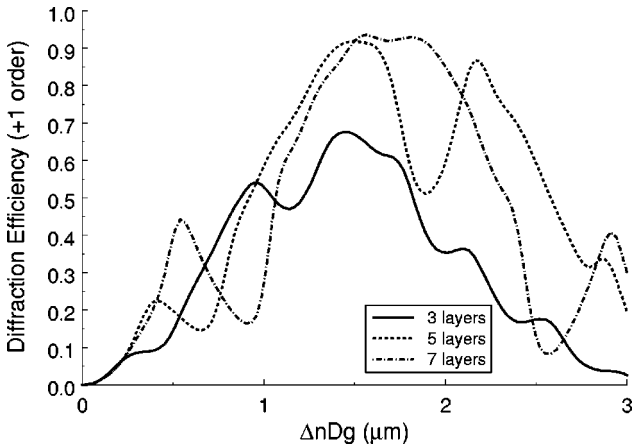

Fig. 4. Diffraction efficiency of a five-layer SVDOE as a function of total grating layer thickness ($\Delta n = 0.5$). $\lambda_0 = 2.06$ μm, θ=9.885°, $n_{\text{I}} = 1.5$, $n_{\text{III}} = 1.5$, $n_{\text{ridge}} = 2.0$, $n_{\text{groove}} = 1.5$, $d_{\text{homogeneous}} = 4.6$ μm.

$$c_R = \cos\,\theta,$$

$$c_S = \cos\,\theta - \frac{\lambda_0}{n\Lambda}\cos\,\phi, \tag{2}$$

where θ is the incidence angle and ϕ is the angle that the grating vector, which is oriented perpendicularly to the fringe planes, makes with the inward surface normal. Also, Λ represents the grating period. The first-order diffraction efficiency as a function of grating parameter χ is given by $\sin^2(\chi)$, and hence it reaches a maximum value when $\chi = \pi/2$.[21] We can use this relationship to determine the optimum modulation thickness for a given sinusoidal refractive index modulation, Δn_{amp}.

We can establish a similar relationship for SVDOE's by realizing that the rectangular refractive-index profile of the binary gratings can be expressed as a sum of sinusoidal refractive-index profiles through a Fourier series:

$$n(x) = n_0 + \sum_{\substack{h=-\infty \\ h\neq 0}}^{h=\infty} \Delta n_h \exp\left(jh\frac{2\pi}{\Lambda}x\right), \tag{3}$$

in which n_0 is the average refractive index of the profile and Δn_h is the amplitude of the hth-harmonic component of the refractive index. A grating parameter can therefore be expressed for SVDOE's by use of the amplitude of the first-harmonic component of the refractive index, which then leads to the relation

$$\chi_{\text{SVDOE}} = \frac{2\pi|\Delta n_1| D_g}{\lambda_0 \sqrt{c_R c_S}}, \tag{4}$$

in which the factor of 2 arises from the exponential expression of the harmonic rather than from the sinusoidal expression that is typical of holographic materials. The dependence of the SVDOE diffraction efficiency on χ_{SVDOE} is therefore $\sin^2(\chi_{\text{SVDOE}})$, so we again reach a peak value of diffraction efficiency when the argument is equal to $\pi/2$. Calculation of Δn_1 in terms of the refractive-index difference between grating ridge and groove materials, Δn, leads to $\Delta n_1 = \Delta n/\pi$. Setting Eq. (4) equal to $\pi/2$ and solving for D_g yields the following expression for the total grating thickness that achieves the maximum diffraction efficiency:

$$D_{g,\max} = \pi \frac{\lambda_0}{4\Delta n}\sqrt{c_R c_S}. \tag{5}$$

Note that calculating $\Delta n D_{g,\max}$ with Eq. (5) for the cases shown in Figs. 3 and 4 leads to a value of 1.51 μm, which is consistent with what is observed in the figures.

Having established the dependence of SVDOE diffraction efficiency on total grating thickness, we proceed to examine SVDOE behavior as a function of homogeneous layer thickness. For the following simulation results we assume five grating layers with a total grating thickness such that $\chi_{\text{SVDOE}} = \pi/2$ for each value of Δn. Figure 5 shows the diffraction efficiency behavior as the thickness of the homogeneous layer between successive grating layers is increased for the case of incidence at the Bragg angle. The +1-order diffraction efficiency is plotted as a function of the sum of a single grating layer thickness and

a single homogeneous layer thickness. Note that the curves are periodic for both $\Delta n = 0.1$ and $\Delta n = 0.5$. Previous research with SVHOE's[11] showed the same type of periodic behavior of the diffraction efficiency as a function of the sum of the homogeneous and the grating layer thicknesses. Also note from Fig. 5 that the curve for $\Delta n = 0.1$ is smoothly varying, whereas the $\Delta n = 0.5$ case exhibits rapid fluctuations that are due, again, to interference from multiple reflections from the grating layers.[22]

Finally, in Fig. 6 we examine the +1-order diffraction efficiency of SVDOE's as a function of the readout beam's incidence angle. A structure consisting of five grating layers with $\Delta n = 0.5$ is assumed. Note that the angular sensitivity exhibits high diffraction efficiency for distinct incidence angles, similar to the behavior of SVHOE's.[10–12] However, there are several differences. First, in previous SVHOE studies it was assumed that the small-angle approximation was valid in the derivation of the incidence angles at which high diffraction efficiency should occur.[11]

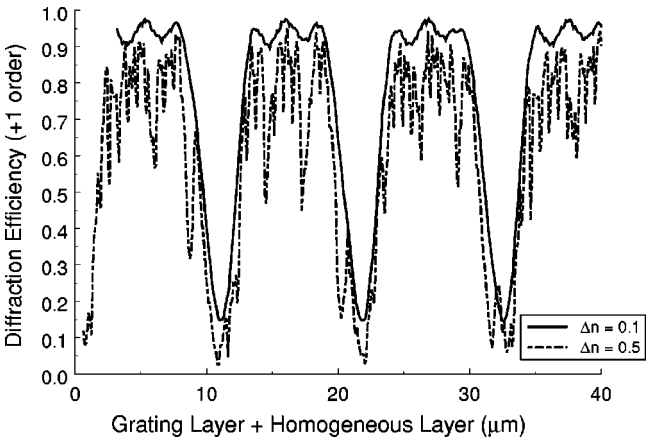

Fig. 5. Diffraction efficiency of a five-layer SVDOE as a function of the thickness of one period in the SVDOE structure (i.e., the sum of a single grating layer thickness and a single homogeneous layer thickness). $\lambda_0 = 2.06$ μm, θ=9.885°, $n_{\mathrm{I}} = 1.5$, $n_{\mathrm{III}} = 1.5$, $n_{\mathrm{groove}} = 1.5$. For $\Delta n = 0.1$, $n_{\mathrm{ridge}} = 1.6$ and $d_{\mathrm{grating}} = 3.139$ μm; for $\Delta n = 0.5$, $n_{\mathrm{ridge}} = 2.0$ and $d_{\mathrm{grating}} = 0.638$ μm.

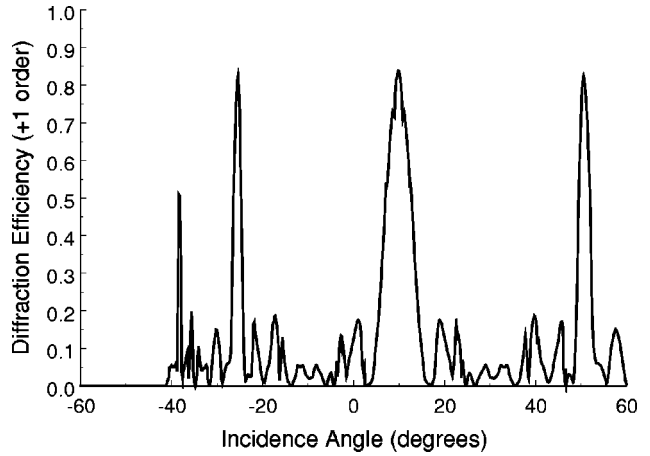

Fig. 6. Angular selectivity of a five-layer SVDOE with $\Delta n = 0.5$. Note that, for $\theta_{\mathrm{inc}} < -41°$, the +1 order is evanescent and hence the diffraction efficiency is zero. $\lambda_0 = 2.06$ μm, $n_{\mathrm{I}} = 1.5$, $n_{\mathrm{III}} = 1.5$, $n_{\mathrm{ridge}} = 2.0$, $n_{\mathrm{groove}} = 1.5$, $d_{\mathrm{grating}} = 0.638$ μm, $d_{\mathrm{homogeneous}} = 4.9$ μm.

This approximation led to a strictly periodic angular sensitivity. In our case, this approximation is not valid; when it is removed from the derivation of Ref. 11 one obtains the following transcendental equation for the angles θ_p at which high diffraction efficiency should occur:

$$\cos\,\theta_p = \left[1 - \left(\sin\,\theta_p - \frac{\lambda_0}{n\Lambda}\right)^2\right]^{1/2} - \frac{p\lambda_0}{d_b n}, \qquad (6)$$

in which d_b is the combined thickness of a single grating layer and a single homogeneous layer and p is an integer (..., −2, −1, 0, 1, 2,...) that distinguishes discrete incidence angles associated with diffraction peaks; e.g., $p = 0$ represents Bragg incidence. Equation (6) accurately predicts the location of the diffraction peaks that occur in Fig. 6.

A second set of differences relative to previously reported SVHOE behavior is due to interference between multiple reflections generated by the large refractive-index difference in the grating layers. For example, one of the expected diffraction peaks shown in Fig. 6 (near −38°) has reduced diffraction efficiency compared with that of the other peaks. This turns out to be a sensitive function of the homogeneous layer thickness when Δn is large. In addition, the sidelobe structure between the main diffraction peaks in Fig. 6 does not exhibit $N - 2$ sidelobes, as is typical for SVHOE's.[10–12] For the case of SVDOE's, we have observed $N - 2$ sidelobes only when Δn was of the order of 10^{-2} or less, and hence there are minimal reflections between grating layers.

3. DESIGN PROCESS

A systematic design process for SVDOE's has been developed based on the diffraction properties discussed in Section 2. The necessary parameters for a complete design include selection of materials (and hence of refractive indices), grating period (which is presumably set by the application), thickness of the grating layers, thickness of the homogeneous layers, and the offset required between adjacent grating layers to achieve high diffraction efficiency at the desired incidence angle. For purposes of this paper, we assume that the grating grooves and the homogeneous layers are composed of the same material and that they hence have the same refractive index.

As discussed in Subsection 2.C, the total grating thickness for a SVDOE can be calculated by use of Eq. (5) once the grating layer's refractive-index difference is known. Likewise, one can calculate the grating layer offsets for a given incidence angle by determining the slant angles for fringes in an equivalent volume grating. The number of grating layers and the homogeneous layer thickness needed to meet a particular diffraction efficiency requirement must be determined numerically with RCWA, which can be accomplished with the following procedure:

1. Divide the total grating thickness into a small number of grating layers.

2. Numerically determine the +1-order diffraction efficiency as a function of the homogeneous layer thickness as shown in Fig. 5 for the desired input beam's incidence angle. For high diffraction efficiency, the grating layers

must be appropriately offset as described above for each homogeneous layer thickness value used in the simulation.

3. From the resultant curve, determine a homogeneous layer thickness that gives high diffraction efficiency.

4. If this diffraction efficiency is not large enough, return to step 1 and increment the number of grating layers, and repeat steps 2 and 3 until a design is achieved that meets the desired diffraction efficiency requirement.

5. Determine the fabrication feasibility of the resultant design and evaluate its robustness relative to likely fabrication-dependent parameter variations.

4. DESIGN FOR LIDAR SCANNER APPLICATION

We applied the above design process to the lidar beam scanner application discussed in Section 1. The specific wavelength of 2.06 μm was chosen because that wavelength was under consideration during initial instrument planning.[23] Candidate homogeneous layer and grating groove materials are expected to have a refractive index of approximately 1.5. Since there are a number of material choices for the grating ridges that have suitable

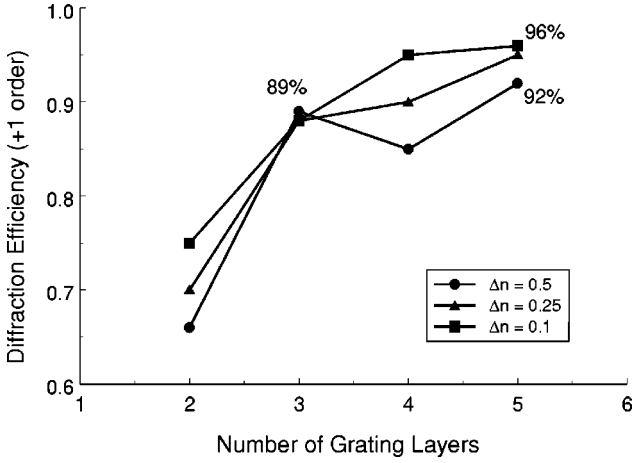

Fig. 7. Diffraction efficiency as a function of number of grating layers. $\lambda_0 = 2.06$ μm, θ=0°, $n_{\mathrm{I}} = 1.5$, $n_{\mathrm{III}} = 1.5$, $n_{\mathrm{groove}} = 1.5$. For $\Delta n = 0.5$, $n_{\mathrm{ridge}} = 2.0$; for $\Delta n = 0.25$, $n_{\mathrm{ridge}} = 1.75$; for $\Delta n = 0.1$, $n_{\mathrm{ridge}} = 1.6$.

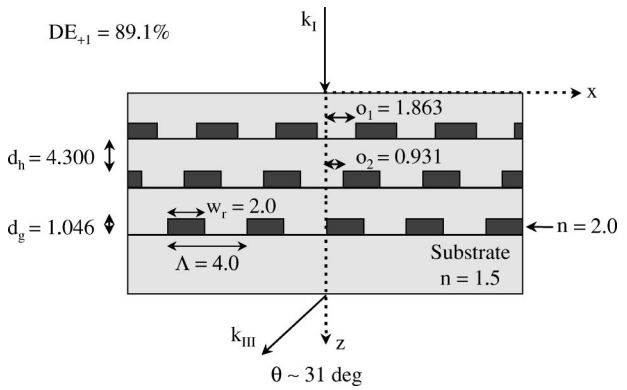

Fig. 8. Specifications for prototype design of a lidar scanner element.

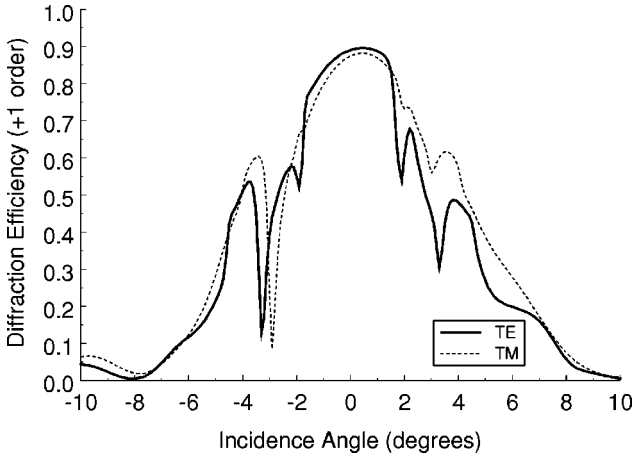

Fig. 9. Diffraction efficiency as a function of incidence angle for both TE and TM polarizations. Three grating layers, $\lambda_0 = 2.06$ μm, $\theta = 0°$, $n_{\mathrm{I}} = 1.5$, $n_{\mathrm{III}} = 1.5$, $n_{\mathrm{ridge}} = 2.0$, $n_{\mathrm{groove}} = 1.5$, $d_{\mathrm{grating}} = 1.046$ μm, $d_{\mathrm{homogeneous}} = 4.300$ μm.

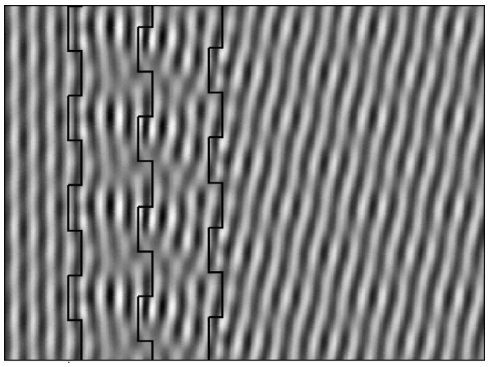

Fig. 10. RCWA representation of the electric field as it traverses the SVDOE prototype lidar scanner. Three grating layers, $\lambda_0 = 2.06$ μm, θ=0°, $n_{\mathrm{I}} = 1.5$, $n_{\mathrm{III}} = 1.5$, $n_{\mathrm{ridge}} = 2.0$, $n_{\mathrm{groove}} = 1.5$, $d_{\mathrm{grating}} = 1.046$ μm, $d_{\mathrm{homogeneous}} = 4.300$ μm.

transmission properties at 2.06 μm, we evaluated designs with grating ridge refractive indices of 1.6, 1.75, and 2.0, yielding Δn values of 0.1, 0.25, and 0.5, respectively. For each Δn, the total grating thickness was calculated with Eq. (5). The grating period was chosen to be 4 μm.

Figure 7 illustrates the results of applying steps 1–4 from Section 3 for each value of Δn. The diffraction efficiency is shown as a function of the number of grating layers parameterized by Δn. For each point in the graph, the homogeneous layer determined in step 3 was selected as the smallest layer thickness that yielded the maximum achievable diffraction efficiency. Also, since the scanner element must operate at normal incidence, the grating ridges were appropriately shifted. Note that the peak diffraction efficiency for the case of two binary grating layers was between 65% and 75%, while in the case of three layers it increased to 89%, regardless of the Δn value. The case of five grating layers was dependent on Δn, yielding a peak efficiency ranging from 92% to 96%.

A diffraction efficiency of ~85% is adequate for our first demonstration device. From Fig. 7 we can see that an element with three grating layers meets that criterion. Also, since an element with three layers requires fewer fabrication steps than one with five layers, we chose to

concentrate on a three-grating-layer design. Likewise, fabrication issues dictate selection of the grating ridge material such that $\Delta n = 0.5$, because this leads to physically thinner grating layers. Thinner layers in turn imply a reduced grating ridge aspect ratio (i.e., grating thickness divided by the ridge width), which is more easily fabricated than larger aspect ratio features.

Geometric specifications for the three-grating-layer structure with $\Delta n = 0.5$, designed for normal incidence, are illustrated in Fig. 8. The SVDOE is implemented upon a substrate that also has a refractive index of 1.5. Each grating layer is 1.046 μm thick, the homogeneous layers are each 4.300 μm thick, and the offset increment between adjacent grating layers is 0.931 μm. A cover layer is shown on top of the SVDOE to protect the features on the uppermost grating. The RCWA prediction of diffraction efficiency in the first diffracted order for a beam normally incident is 89.1%.

The lidar beam incident upon the scanner will be circularly polarized. For optimum performance of the lidar's heterodyne detection scheme, that polarization must be maintained as the beam traverses the scanner element. This implies that diffraction efficiency must be insensitive to polarization of the incident beam. Figure 9 shows the diffraction efficiency as a function of the input beam's incidence angle for the three-grating-layer structure. Note that the efficiency remains greater than 85% in a region of $\pm 1°$ about normal incidence for both TE and TM polarization. The broad peak about normal incidence provides misalignment tolerance when the element is placed in the lidar system.

Our implementation of the RCWA simulation yields an expression for the electric and magnetic fields as they traverse the SVDOE structure. Figure 10 is a representation of the electric field in the three-layer prototype lidar scanner element design considered here. A plane wave is shown entering the SVDOE at normal incidence from the left of the figure. Small interference effects between the incident and the reflected waves can be seen in the incident region. As the wave fronts pass through the first grating layer they are slightly disrupted, whereas passing through the second grating layer causes them to become completely fractured. The third grating layer connects a lagging wave front with a leading wave front to effect the redirection of the beam to the desired deflection angle. The exiting medium in this figure is the substrate, with a refractive index of 1.5.

Anticipated challenges in fabricating a SVDOE include accurate alignment of the grating layers to achieve the desired layer-to-layer offset and deposition of the homogeneous layers with the desired thickness. To assess the tolerances required for these parameters during fabrication we performed a statistical study of the effects of zero-mean Gaussian random deviations of each parameter from the design values. The effects of these variations on diffraction efficiency of the three-grating-layer prototype lidar scanner element are shown in Figs. 11 and 12. In Fig. 11 the solid curve represents the average diffraction efficiency as a function of the standard deviation of the additive random Gaussian variation of the grating offsets and the dotted curve is the standard deviation of the diffraction efficiency. The grating layer offsets must be aligned within approximately 30 nm of their design position to maintain a diffraction efficiency above 85%. Figure 12 is similar to Fig. 11 but addresses variation of homogeneous layer thicknesses. From this figure it is apparent that the tolerance on homogeneous layer thickness is not so critical as the grating offset accuracy to maintain a high diffraction efficiency.

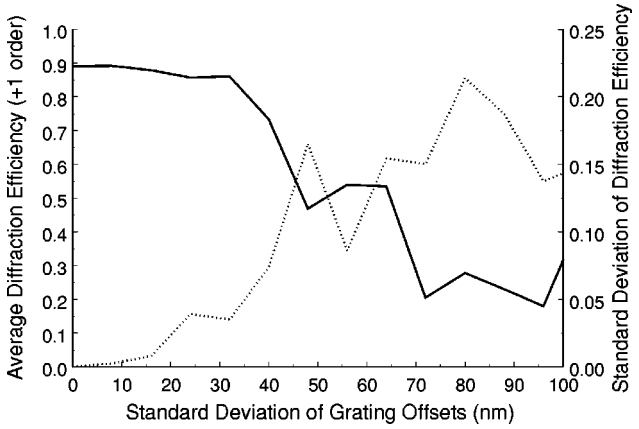

Fig. 11. Effect of statistical variation of grating layer offsets on the diffraction efficiency of the prototype lidar scanner. Three grating layers, $\lambda_0 = 2.06$ μm, θ=0°, $n_{\mathrm{I}} = 1.5$, $n_{\mathrm{III}} = 1.5$, $n_{\mathrm{ridge}} = 2.0$, $n_{\mathrm{groove}} = 1.5$, $d_{\mathrm{grating}} = 1.046$ μm, $d_{\mathrm{homogeneous}} = 4.300$ μm.

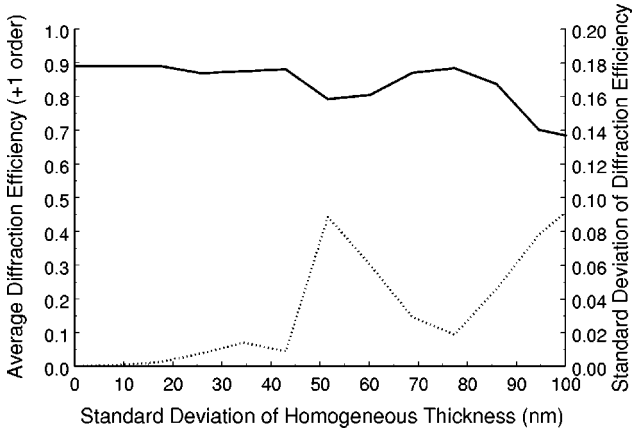

Fig. 12. Effect of statistical variation of homogeneous layer thickness on the diffraction efficiency of the prototype lidar scanner. Three grating layers, $\lambda_0 = 2.06$ μm, θ=0°, $n_{\mathrm{I}} = 1.5$, $n_{\mathrm{III}} = 1.5$, $n_{\mathrm{ridge}} = 2.0$, $n_{\mathrm{groove}} = 1.5$, $d_{\mathrm{grating}} = 1.046$ μm, $d_{\mathrm{homogeneous}} = 4.300$ μm.

5. SUMMARY AND FUTURE RESEARCH

The use of stratified volume diffractive optical elements (SVDOE's) has been proposed as a way to create high-efficiency gratings for applications with requirements that are not suited to traditional volume holographic or diffractive optic techniques. An example application has been studied to illustrate a set of operational and performance requirements that may be best met by a SVDOE structure that emulates volume grating behavior. A modeling algorithm based on RCWA has been developed, and an example SVDOE structure for the coherent wind

lidar application has been presented. This design yielded a predicted diffraction efficiency of 89.1%.

Our future efforts with SVDOE's will initially be directed toward fabricating and experimentally validating our models and design techniques. As mentioned above, challenges in fabricating these elements will include developing processes that allow the design to be produced within the tolerances necessary to achieve high diffraction efficiency. The first generation of demonstration elements will have an aperture diameter of 5.08 cm (2 in.). Future elements will explore scale-up issues in expanding the aperture to the full diameter required by operational lidar systems.

APPENDIX A

In this appendix we illustrate the implementation of a stable and efficient RCWA algorithm encompassing both grating and homogeneous layers for the specific case of planar diffraction with TE polarization. It is straightforward to extend the algorithm to TM-mode planar diffraction and conical diffraction. We closely follow the formulation presented by Moharam *et al.*[15,16] in which the tangential fields are expressed as a Fourier expansion in terms of space harmonics and then electromagnetic boundary conditions are applied at each layer in the structure. The expressions for the boundary conditions are written in matrix form, and transmittance matrix methods are applied to reduce the system of equations to a single matrix equation encompassing all layers. Finally, enhanced transmittance matrix methods are applied to ensure that the matrix equation can be solved without numerical instabilities.

In the formulation shown here, a linearly polarized beam is obliquely incident upon a grating structure. The beam is oriented such that planar diffraction occurs and its polarization is in TE mode. The geometry of this configuration is shown in Fig. 1 for normal incidence; for oblique incidence the propagation vector k_{I} forms an angle θ with respect to the z axis in the plane of the figure. Expressions for the electric fields in the incident and transmitted regions for these conditions are given in Eqs. (4) and (5) and expressions for the propagation vectors are given in Eqs. (6) and (7) of Ref. 15.

We begin here with Eqs. (9) and (10) of Ref. 15, in which the tangential electric (y-component) and tangential magnetic (x-component) fields are expressed in a grating region with a Fourier expansion in terms of the space-harmonic fields. We then apply an additional subscript to differentiate among grating layers [as in Eq. (19) of Ref. 16 for the case of TM polarization], and the tangential field expressions become

$$E_{l,y} = \sum_{i=-\infty}^{\infty} S_{l,yi}(z)\exp(-jk_{xi}x), \tag{A1}$$

$$H_{l,x} = -j\left(\frac{\epsilon_0}{\mu_0}\right)^{1/2} \sum_{i=-\infty}^{\infty} U_{l,xi}(z)\exp(-jk_{xi}x), \tag{A2}$$

in which z is the distance through the grating layer along the z axis [e.g., Eq. (15) of Ref. 16] and all other symbols are described in Refs. 15 and 16.

Continuing as in Eqs. (17) and (18) of Ref. 15 and applying the multilayer notation again, we then find the space harmonics of the tangential electric and magnetic fields in the grating layers to be

$$S_{l,yi}(z) = \sum_{m=1}^{n} w_{l,i,m}\{c_{l,m}{}^{+}\exp[-k_0 q_{l,m}(z - D_{l-1})] + c_{l,m}{}^{-}\exp[k_0 q_{l,m}(z - D_l)]\}, \tag{A3}$$

$$U_{l,xi}(z) = \sum_{m=1}^{n} v_{l,i,m}\{-c_{l,m}{}^{+}\exp[-k_0 q_{l,m}(z - D_{l-1})] + c_{l,m}{}^{-}\exp[k_0 q_{l,m}(z - D_l)]\}, \tag{A4}$$

where D is defined in Eq. (15) of Ref. 16. Similarly, the space harmonics of the tangential electric and magnetic fields in the homogeneous layers can be expressed as

$$S_{l,yi}(z) = P_{l,i}\exp[-k_0\gamma_{l,i}(z - D_{l-1})] + Q_{l,i}\exp[k_0\gamma_{\gamma,i}(z - D_l)], \tag{A5}$$

$$U_{l,xi}(z) = -\gamma_{l,i}P_{l,i}\exp[-k_0\gamma_{l,i}(z - D_{l-1})] + \gamma_{l,i}Q_{l,i}\exp[k_0\gamma_{l,i}(z - D_l)], \tag{A6}$$

where all symbols are defined as in Ref. 16, with the exception of γ, which is defined as

$$\gamma_{l,i} = j\left[n_l{}^2 - \left(\frac{k_{xi}}{k_0}\right)^2\right]^{1/2}. \tag{A7}$$

Equations (A3)–(A6) for space harmonics in both grating and homogeneous layers are written in matrix form, and the electromagnetic boundary conditions are applied between successive layers and also between the uppermost layer and the incident region and the lowermost layer and the transmitted region. First, consider the space harmonics for the grating layers. Equation (A3) and (A4) can be written in matrix form to represent the electromagnetic boundary conditions at the upper boundary for a particular grating layer, e.g., $z = D_{l-1}$:

$$\begin{bmatrix} S_{l,y} \\ U_{l,x} \end{bmatrix}_{Z = D_{l-1}} = \begin{bmatrix} W_l & W_l X_l \\ V_l & -V_l X_l \end{bmatrix}\begin{bmatrix} C_l{}^{+} \\ C_l{}^{-} \end{bmatrix}, \tag{A8}$$

or at the lower boundary for that layer, e.g., $z = D_l$:

$$\begin{bmatrix} S_{l,y} \\ U_{l,x} \end{bmatrix}_{Z = D_l} = \begin{bmatrix} W_l X_l & W_l \\ V_l X_l & -V_l \end{bmatrix}\begin{bmatrix} C_l{}^{+} \\ C_l{}^{-} \end{bmatrix}, \tag{A9}$$

in which W_l is the eigenvector matrix that results from the coupled-wave equations in that layer, $V_l = W_l Q_l$, where Q_l is a diagonal matrix whose elements are the eigenvalues, X_l is a diagonal matrix with elements $\exp(-k_0 q_{l,m} d)$, where d is the thickness of the grating layer, and $C_l{}^{+,-}$ are the unknown coefficients.

Similarly, the boundary conditions at the upper and lower boundaries of a homogeneous layer can be written in matrix form by use of Eqs. (A5) and (A6). For example,

$$\begin{bmatrix} S_{l,y} \\ U_{l,x} \end{bmatrix}_{Z = D_{l-1}} = \begin{bmatrix} I & IG_l \\ \Gamma_l & -\Gamma_l G_l \end{bmatrix}\begin{bmatrix} P_l \\ Q_l \end{bmatrix}, \tag{A10}$$

$$\begin{bmatrix} S_{l,y} \\ U_{l,x} \end{bmatrix}_{Z = D_l} = \begin{bmatrix} IG_l & I \\ \Gamma_l G_l & -\Gamma_l \end{bmatrix} \begin{bmatrix} P_l \\ Q_l \end{bmatrix}, \tag{A11}$$

in which I is an identity matrix, G_l is a diagonal matrix with elements $\exp(-k_0 \gamma_{l,i} d)$, where d is the thickness of the homogeneous layer, Γ_l is a diagonal matrix with elements γ_l, and $P_l$and Q_l are unknown coefficients.

On examination of Eqs. (A8) and (A10) it is apparent that a similar matrix representation arises at the upper boundary of a layer, regardless of whether it is a grating or a homogeneous layer. This can be written in general notation as

$$\begin{bmatrix} S_{l,y} \\ U_{l,x} \end{bmatrix}_{Z=D_{l-1}} = \begin{bmatrix} A_{l,1} & A_{l,1}\Omega_l \\ A_{l,2} & -A_{l,2}\Omega_l \end{bmatrix} \begin{bmatrix} \rho_{l,1} \\ \rho_{l,2} \end{bmatrix}, \tag{A12}$$

in which $A_{l,1}$ represents either W_l or I as appropriate, $A_{l,2}$ represents V_l or Γ_l, Ω_l represents the exponential functions X_l or G_l,and ρ_l represents the coefficients $C_l^{+,-}$ or P_l, Q_l. Similarly, Eqs. (A9) and (A11) can be written as a general representation at the lower boundary of a layer as

$$\begin{bmatrix} S_{l,y} \\ U_{l,x} \end{bmatrix}_{Z=D_l} = \begin{bmatrix} A_{l,1}\Omega_l & A_{l,1} \\ A_{l,2}\Omega_l & -A_{l,2} \end{bmatrix} \begin{bmatrix} \rho_{l,1} \\ \rho_{l,2} \end{bmatrix}. \tag{A13}$$

Now that a general notation has been determined for all layers, the boundary conditions for the electric and the magnetic fields are matched at each layer interface from the incident region, through the optical structure and into the transmitted region. By applying the transmittance matrix approach one can reduce the system of equations to a general representation as

$$\begin{bmatrix} \delta_{i,0} \\ jn_{\mathrm{I}} \cos\theta\delta_{i,0} \end{bmatrix} + \begin{bmatrix} I \\ -jY_{\mathrm{I}} \end{bmatrix} R = \prod_{l=1}^{L} \begin{bmatrix} A_{l,1} & A_{l,1}\Omega_l \\ A_{l,2} & -A_{l,2}\Omega_l \end{bmatrix} \times \begin{bmatrix} A_{l,1}\Omega_l & A_{l,1} \\ A_{l,2}\Omega_l & -A_{l,2} \end{bmatrix}^{-1} \begin{bmatrix} I \\ jY_{\mathrm{III}} \end{bmatrix} T, \tag{A14}$$

in which R, T, and Y are defined in Ref. 16. Equation (A14) is similar to Eq. (27) of Ref. 16, specific to the case of TM polarization. In this formulation the ordering of grating and homogeneous layers may be arbitrary but still satisfy Maxwell's equations throughout the system. Applying the enhanced transmittance matrix approach yields the expression

$$\begin{bmatrix} \delta_{i,0} \\ jn_{\mathrm{I}} \cos\theta\delta_{i,0} \end{bmatrix} + \begin{bmatrix} I \\ -jY_{\mathrm{I}} \end{bmatrix} R = \begin{bmatrix} A_{1,1}(1 + \Omega_1 b_1 a_1^{-1}\Omega_1) \\ A_{1,2}(I - \Omega_1 b_1 a_1^{-1}\Omega_1) \end{bmatrix} T_1, \tag{A15}$$

where

$$T = a_L^{-1}\Omega_L a_{L-1}^{-1}\Omega_{L-1} \ldots a_2^{-1}\Omega_2 a_1^{-1}\Omega_1 T_1, \tag{A16}$$

in which a and b are defined in Ref. 16. Equations (A15) and (A16) are similar to Eqs. (31) and (32) of Ref. 16. This expression can be solved for R and T by standard techniques of linear algebra.

ACKNOWLEDGMENTS

D. M. Chambers was supported for this effort under contract NAS8-40836 with the NASA/Marshall Space Flight Center, with funding provided by Michael J. Kavaya. G. P. Nordin was supported by National Science Foundation CAREER award ECS-9625040. The authors gratefully acknowledge many helpful discussions with Farzin Amzajerdian of the Center for Applied Optics, University of Alabama in Huntsville.

*When this research was performed, D. M. Chambers was employed by Micro Craft, Inc., 620 Discovery Drive, Huntsville, Alabama 35806. D. M. Chambers can be reached at the address on the title page or by e-mail at chambers@email.uah.edu.

REFERENCES

1. L. Solymar and D. J. Cooke, *Volume Holography and Volume Gratings* (Academic, New York, 1981).
2. M. B. Fleming and M. C. Hutley, "Blazed diffractive optics," Appl. Opt. **36**, 4635–4643 (1997).
3. D. C. O'Shea and W. S. Rockward, "Gray-scale masks for diffractive-optics fabrication. II. Spatially filtered halftone screens," Appl. Opt. **34**, 7518–7526 (1995).
4. T. J. Suleski and D. C. O'Shea, "Gray-scale masks for diffractive-optics fabrication. I. Commercial slide imagers," Appl. Opt. **34**, 7507–7517 (1995).
5. W. Daschner, P. Long, R. Stein, C. Wu, and S. H. Lee, "Cost-effective mass fabrication of multilevel diffractive optical elements by use of a single optical exposure with a gray-scale mask on high-energy beam-sensitive glass," Appl. Opt. **36**, 4675–4680 (1997).
6. J. M. Miller, N. De Beaucoudrey, P. Chavel, J. Turunen, and E. Cambril, "Design and fabrication of binary slanted surface-relief gratings for a planar optical interconnection," Appl. Opt. **36**, 5717–5727 (1997).
7. Z. Zhou and T. J. Drabik, "Optimized binary, phase-only diffractive optical element with subwavelength features for 1.55 μm," J. Opt. Soc. Am. A **12**, 1104–1112 (1995).
8. M. W. Farn, "Binary gratings with increased efficiency," Appl. Opt. **31**, 4453–4458 (1992).
9. M. C. Gupta and S. T. Peng, "Diffraction characteristics of surface-relief gratings," Appl. Opt. **32**, 2911–2917 (1993).
10. R. V. Johnson and A. R. Tanguay, Jr., "Stratified volume holographic optical elements," Opt. Lett. **13**, 189–191 (1988).
11. G. P. Nordin, R. V. Johnson, and A. R. Tanguay, Jr., "Diffraction properties of stratified volume holographic optical elements," J. Opt. Soc. Am. A **9**, 2206–2217 (1992).
12. G. P. Nordin and A. R. Tanguay, Jr., "Photopolymer-based stratified volume holographic optical elements," Opt. Lett. **17**, 1709–1711 (1992).
13. F. Amzajerdian and M. J. Kavaya, "Development of solid state coherent lidars for global wind measurements," presented at the Ninth Conference on Coherent Laser Radar, June 23–27, 1997, Linkoping, Sweden.
14. A. Granger, L. Song, and R. A. Lessard, "Multiple beam generation using a stratified volume holographic grating," Appl. Opt. **32**, 2534–2537 (1993).
15. M. G. Moharam, E. B. Grann, D. A. Pommet, and T. K. Gaylord, "Formulation for stable and efficient implementation of the rigorous coupled-wave analysis of binary gratings," J. Opt. Soc. Am. A **12**, 1068–1076 (1995).
16. M. G. Moharam, D. A. Pommet, E. B. Grann, and T. K. Gaylord, "Stable implementation of the rigorous coupled-wave analysis for surface-relief gratings: enhanced transmittance matrix approach," J. Opt. Soc. Am. A **12**, 1077–1086 (1995).
17. M. G. Moharam and T. K. Gaylord, "Rigorous coupled-wave

analysis of planar-grating diffraction," J. Opt. Soc. Am. **71**, 811–818 (1981).
18. M. G. Moharam and T. K. Gaylord, "Diffraction analysis of dielectric surface-relief gratings," J. Opt. Soc. Am. **72**, 1385–1392 (1982).
19. L. Li, "Use of Fourier series in the analysis of discontinuous periodic structures," J. Opt. Soc. Am. A **13**, 1870–1876 (1996).
20. S. Tibuleac and R. Magnusson, "Reflection and transmission guided-mode resonance filters," J. Opt. Soc. Am. A **14**, 1617–1626 (1997).
21. H. Kogelnik, "Coupled wave theory for thick hologram gratings," Bell Syst. Tech. J. **48**, 2909–2947 (1969).
22. J. J. Jung, "Stratified volume holographic optical elements: analysis of diffraction behavior and implementation using InGaAs/GaAs multiple quantum well structures," Ph.D. dissertation (University of Southern California, Los Angeles, Calif., 1994).
23. F. Amzajerdian, Center for Applied Optics, The University of Alabama in Huntsville, Huntsville, Ala. 35899 (personal communication, 1996).